Experiments on the Distributions of Local Pressure and Heat Transfer on a Grid Simulating a Parachute Fabric

C. J. Scott* and M. Ruiz-Urbieta†
University of Minnesota, Minneapolis, Minn.

This paper describes the methods and results of an experimental program to determine the pressure and heat-transfer distributions to an individual fiber of a porous parachute designed to decelerate vehicles from supersonic velocities. An enlarged scale model of the woven mesh was studied in which the simulated fibers were 1 in. in diameter. The geometric porosity of the grid was 25%. A blowdown wind tunnel served as the flow facility. The average velocity of the approaching airflow was 134 fps. The pressure ratio applied across the mesh was considered as the primary variable. Data were taken at six pressure ratios ranging from 11, which was the highest obtainable with the facility used, to 1.5, which was as close to unity as was felt to be of interest. Using a transient energy balance, heating rates to selected fibers were measured. Regions of separated flow covered approximately 70% of the surface area exposed to the flow. Variations in local heat flux were minor such that the average heat transfer to the mesh may be correlated to the forward stagnation point location where theoretical laminar boundary-layer predictions were confirmed.

I. Introduction

A GROWING interest in aerospace vehicle recovery operations has directed attention to a variety of deceleration devices. In certain cases a sizeable portion of the kinetic energy of the forebody is converted into an increase in internal energy of the retardation device, and aerodynamic heat transfer becomes a design factor. Towed decelerators such as ribbon or hyperflo parachutes, balloons, and ballutes have flexible canopies. Other proposals incorporate structural members (cones or paragliders) or hybrid systems such as the Avco drag brake[1] and the NASA rotornet.[2] Aerodynamic decelerators must possess a large drag-to-weight ratio and must be capable of being stored in a small volume. Therefore, most drag-producing devices are relatively thin and flexible. Impermeable retardation devices are aerodynamically unstable when utilized in a supersonic flow. As a result, nearly all of the retardation devices listed above employ extended porous surfaces in conjunction with other venting techniques (see Fig. 1). Most conventional textile fibers either melt or are seriously degraded by exposure to temperatures above 500°F. It is desirable to replace these fibers with materials of higher thermal durability such as fine metallic wires in which operational temperatures are close to 2000°F.

It is felt that for the purpose of analysis the flowfield associated with a porous retardation device includes large-scale phenomena enveloping the entire body and small-scale processes associated with the local flow about a single element in the mesh material itself. The large-scale phenomena such as parachute shape or size and the velocity and altitude involve the external aerodynamics of the problem and contribute the end or boundary conditions (such as pressure ratio or Reynolds number) to the small-scale phenomena.

The geometry under consideration is a porous weave consisting of individual round wire filaments. The flow through a single pore is taken to be analogous to the flow through a nozzle. At supersonic flight speeds and at very high porosities,‡ discrete shock waves form ahead of each cylinder. If the porosity is lower, i.e., insufficient to permit supersonic flow to be "started" in each nozzle in a manner similar to the starting process in a closed-channel wind tunnel, a continuous shock appears ahead of the entire mesh surface. At such intermediate porosities and sufficiently large Reynolds numbers, a discrete boundary layer will form on each cylinder. Only at very low porosities and Reynolds numbers will the individual boundary layers merge to fill the pores completely and establish a continuous boundary layer over the entire mesh surface. Only the intermediate porosity-discrete boundary-layer case will be studied in the present paper.

A. Large-Scale Phenomena

The range of interest in the present study consists of altitudes from sea level up to 200,000 ft and flight Mach numbers ranging from 2 to 5. A concave hemisphere canopy is a typical shape considered for supersonic operations, although specification of the exact geometry is not necessary. In pre-

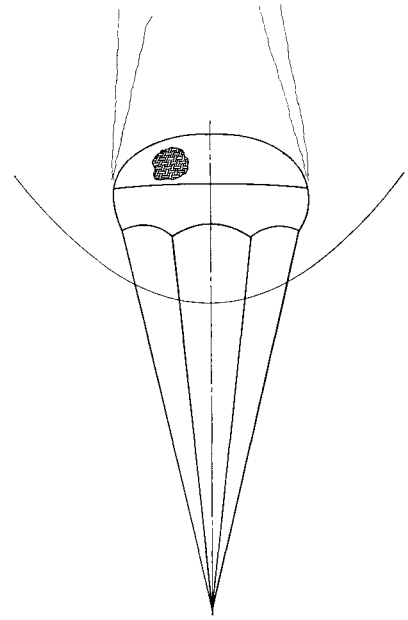

Fig. 1 Sketch of porous parachute.

Received April 13, 1967; revision received September 14, 1967. The research reported in this paper was sponsored by the Recovery and Crew Station Branch of the Air Force Flight Dynamics Laboratory under Contract AF 33(657)11688.

* Associate Professor of Mechnical Engineering.

† Research Assistant, Heat Transfer Laboratory.

‡ Porosity is defined geometrically as the ratio of open area to total area of the forward-facing surface of the retardation device.

vious work,[3] it was felt that a good starting point for study of the large-scale phenomena was the simple concave hemisphere. The experimental results of Ref. 3 indicate that at angular locations up to 75° from the stagnation point, the static pressure on the upstream surface of the concave hemisphere is equal to the total pressure. This means that there is practically no flow near and parallel to the surface of the hemisphere except near the edge. Of course, in supersonic flow, a normal shock would stand ahead of the hemisphere, and this would produce a completely subsonic flow regime inside of the concave hemisphere. In the absence of any parachute porosity, the pressure on the upstream side of the chute is closely approximated by the total pressure behind the normal shock. In determining the pressure on the rearward (downstream) face of the parachute, we are led to a base pressure phenomenon described by H. H. Korst.[4]

The discussion in the previous paragraph illustrates a technique for computing the pressures and, hence, the pressure ratio across a chute with no porosity. The analysis for the base pressure problem has been extended to the case of flow through the chute with small momentum only. Since this last condition is rarely met in the case of practical parachute configurations, the pressure ratio across the chute openings must be found from experiment.

B. Small-Scale Phenomena

A high-temperature, high-density flow is produced inside the canopy. This flow passes through the individual openings of the mesh. Heat is transferred from the hot gases to the mesh elements. Therefore, it is the distribution of heat flux to the surfaces of a mesh element which is of primary importance. The element is bounded on each side by an opening (slot) through which the oncoming flow passes. The typical element may be considered as a cylinder aligned normal to the flow. The approaching flow may or may not separate upstream of the cylinder. This process has not been clearly defined.

The flow passing through the slots exhibits properties that depend upon the over-all applied pressure ratio. In most flight applications, the applied pressure ratio will be such that the flow in the slot may be considered as sonic. Additional energy is available for further expansion of the stream as it emerges from the slot such that localized regions of supersonic flow will occur downstream of the slot. Between the supersonic jets emerging from the slot and the rearward-facing surface of the cylinder, two regions are found. The first is a conventional free-shear layer in which the streamwise component of velocity diminishes from the value found in the jet to a near-zero condition. Adjacent to the shear layer there exists a small region of reverse flow with a circulating vortex. The local pressure in the separation bubble is determined by local base pressure phenomena (the flow issuing from the slot). The mean near-wake pressure which exists further downstream is determined by the gross geometry and the freestream Mach number. These two pressures are generally not equal. Therefore, further recompression exists downstream of the jets issuing from the individual slots. The local base pressure behind an indidividual ribbon is therefore determined by the slot pressure ratio and the recompression process in the jets.

The greatest source of uncertainty in engineering calculations of the energy exchange process to the mesh elements lies in the determination of the convective heat flux as characterized by a heat-transfer parameter Nu, which is a function of a number of parameters. This is expressed by the following dimensionless relationship:

$$Nu = f(Re,M,Kn,T_w/T_0,\text{geometry})$$

The Reynolds number Re describing the flow conditions around the fibers will, in this paper, be based on cylinder

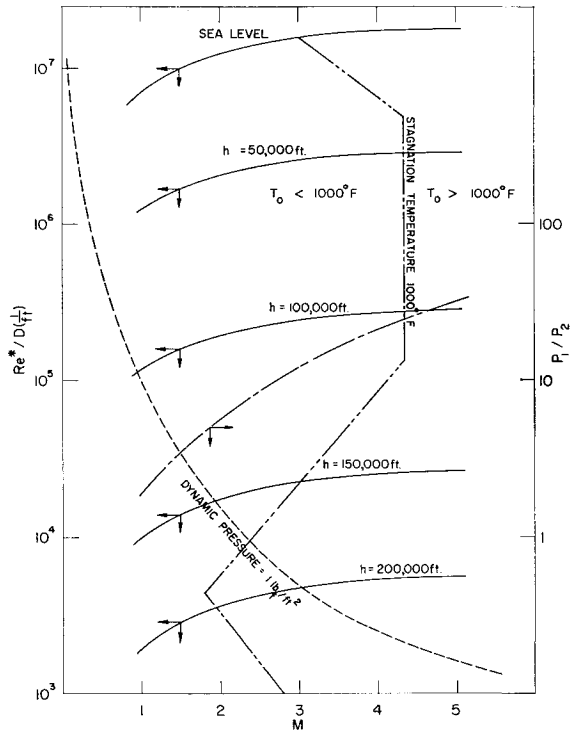

Fig. 2 Unit Reynolds number vs flight Mach number for various flight altitudes.

diameter D and on the average velocity and properties in the flow through the slots between the mesh elements where, for supercritical pressure ratio, sonic velocity exists. This Reynolds number is denoted as $Re^* = Du^*/\nu^*$. In Fig. 2, Re^*/D is plotted vs descent Mach number M for altitudes ranging from sea level to 200,000 ft. This unit Reynolds number is presented since it does not require the specification of a body dimension that varies with a specific parachute. The large values of Re^*/D which exist at low altitudes produce high heat flux rates. The short-dashed curve is a curve of constant dynamic pressure, connected with the descent velocity, of 1 lb per square ft, below which reliable self-inflation of flexible drag devices cannot be expected. The curve labeled "stagnation temperature = 1000°F" illustrates the heat-transfer problem as determined by Mach number effects. The operating regime of conventional parachutes lies within the envelope of the two preceding curves.

The descent Mach number M has only an indirect influence upon the heat transfer to the ribbons insofar as it determines the pressure and temperature both inside the canopy and behind it. For the flow and heat transfer around the ribbons, the pressure ratio p_1/p_2 is a more suitable parameter. Its use has the further advantage that it can be measured readily in a wind-tunnel experiment on a parachute model. The pressure ratio curve presented in Fig. 2 is the ratio of the total pressure behind a normal shock to the freestream static pressure and represents the minimum pressure ratio that should be studied at any simulated flight Mach number.

The Prandtl number Pr, whose value is approximately 0.7 under normal atmospheric conditions, deviates up to ±10% from this value up to temperatures of approximately 6000°R. At altitudes up to 400,000 ft the stagnation temperatures for $M \leq 10$ will be below 6000°R. The deviation of the Prandtl number from the value 0.7 may be neglected.

The Knudsen number Kn will enter as a parameter only at very low densities. It can be expressed as a relation between Mach number and Reynolds number, for instance by $M/(Re)^{1/2}$. In this expression, the mean free path of the molecules is related to the boundary-layer thickness. The determination of the critical value of $M/(Re)^{1/2}$ depends on

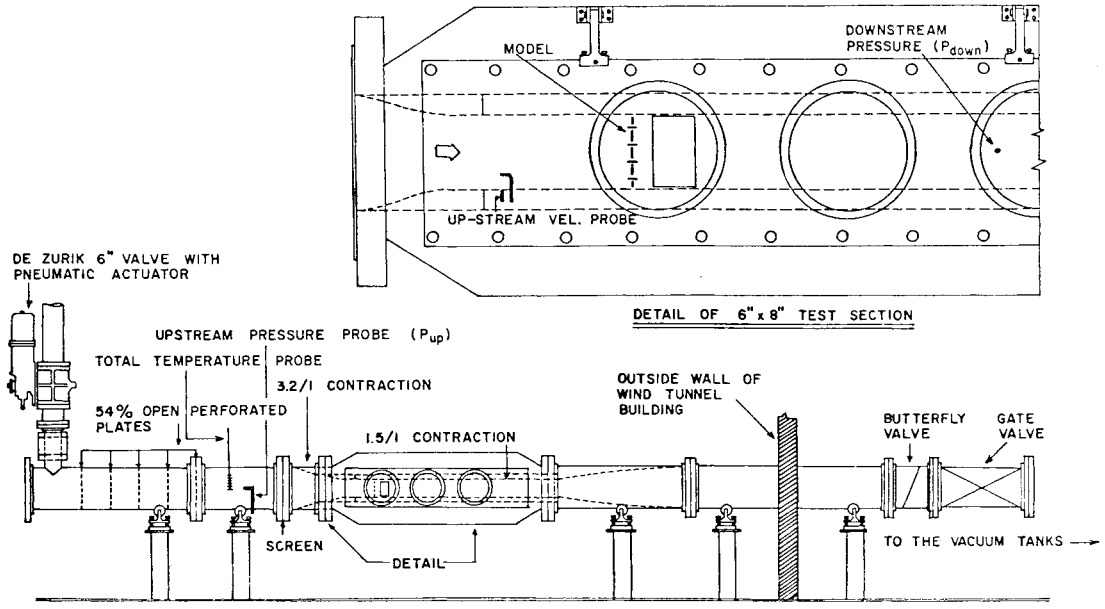

Fig. 3 Sketch of the wind tunnel.

the shape of the body which affects the boundary-layer growth. However, for an approximate evaluation it seems justified to introduce M^* and Re^* as characteristic values for the flow around a ribbon into the Knudsen number. Herman[5] gives as critical value $M^2/Re = 10^{-3}$. In our case, $M^* = 1$. Thus, continuum flow can be expected to exist for descent conditions at which $Re = Re^* > 1000$. The conditions for which this is the case are evident from Fig. 2. The results presented in this paper are valid for the continuum flow regime. Summarizing the foregoing discussion on the influence of the various parameters upon the heat transfer on a parachute fiber, we can expect a relation

$$Nu = f(Re, P_1/P_2)$$

This relation, then, has to be determined by experiments.

It is convenient to define a Reynolds number based on the velocity and flow properties in the sonic orifice and the slot width,

$$Re^*_D = \rho^* a^* D/\mu^* \qquad (1)$$

In the flight case, the static temperature T_∞ and pressure p_∞ are determined by the flight altitude. A total pressure p_0 and temperature T_0 are determined once the flight Mach number is prescribed. Since the bow shock is assumed to be normal, the total pressure behind the normal shock p'_0 (inside the canopy) is determined from P_0 and M_∞.§ The total density, behind the bow shock, is computed from p'_0, T_0 and the proper equation of state. Finally, the sonic density and speed are determined from an isentropic expansion from p'_0, T_0, to p^* and T^*. The superscript * refers to the slot condition where a sonic speed exists for supercritical pressure ratios. The viscosity μ^* is a known function of the temperature T^*.

II. Experimental Equipment and Procedures

A. Facility

The experimental facility used in the present experiments appears in the sketch of the experimental setup, Fig. 3. This facility is located at University of Minnesota's Rosemount Research Center. Prior to modification, the wind tunnel was a conventional blowdown supersonic wind tunnel.[6] The 6- × 12-in. supersonic wind tunnel was modified by removing the supersonic nozzle blocks and fabricating a new 6- × 8-in. inlet pipe. The opening time of this valve is slightly less than 1 sec, which is of importance when transient heat-transfer measurements are made. A series of five perforated plates were placed at 11-in. intervals inside the 18-in.-diam. stilling chamber and a 16-mesh screen was inserted between the flanges at the downstream end of this chamber to even out the flow. The plates and screen had a porosity of about 54%. Test reported by Baines and Peterson[7] indicated that this is an optimum porosity for flattening out nonuniform velocity profiles.

A short round-to-rectangular contraction with an area ratio of 3.2 followed the stilling chamber, and the supersonic nozzle blocks normally were installed immediately downstream. These blocks were replaced by a pair of two-dimensional subsonic contraction blocks with a contraction ratio of 1.5. The contraction contours (cubical arcs) were determined from the data given by Rouse and Hasson[8] on a cavitation prevention basis. The second contraction provided an additional acceleration of the flow to 134 fps. It also served the purpose of reducing the thickness of the nozzle boundary-layer.

Upstream of the test section, the air was taken directly from the atmosphere, and therefore the compressed-air system was not used. Downstream of the model, air was led into the vacuum tanks. The vacuum system has a capacity of 22,750 cubic ft and is evacuated by two Allis-Chalmers 27-D vacuum pumps. These pumps, rated at 3390 cfm each, are powered by a 350 hp motor, which drives both pumps. The lowest vacuum obtainable with the pumps in series was 2 in. Hg.

At the highest pressure ratio, $P_{up}/P_{down} \simeq 11$–$12$, the characteristic running time of the wind tunnel was about 4 min. After this time it was not possible to maintain a constant pressure ratio since the pumping system was not able to pump out the air flowing into the vacuum tanks. Because of this, the downstream pressure started to increase and the pressure ratio decreased. The rate of change of the pressure ratio decreased with decreasing pressure ratio.

For supercritical operations the value of the unit Reynolds number Re^*_D was held constant at a value of 5×10^5. Thus

§ The present experimental procedure is to simulate the subsonic flow conditions behind the bow shock. The total pressure behind the normal shock is properly simulated by the wind-tunnel stagnation pressure.

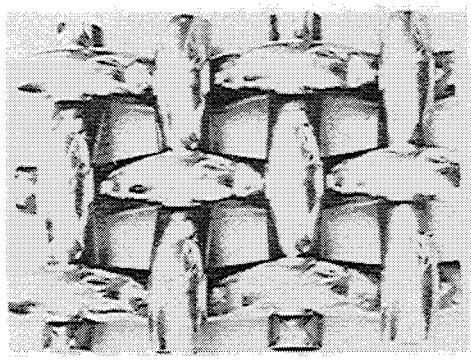

Fig. 4 The test model without supporting pieces.

the pressure ratio is the primary variable in the present experiments.

B. The Experimental Model

A photograph of the test grid is given as Fig. 4. Although a variety of yarn and weave constructions may be practical, the one chosen seems most basic. The model consists of seven highly polished bars milled from solid billets of free-machining stainless steel and arranged in such a way that they resemble woven cloth of 25% geometric porosity. Stainless steel was chosen because of its relatively small thermal conductivity and its corrosion resistance. It should be recalled, however, that since only the rate of heat transfer through the air to the surface is being considered, the material used in the model can be chosen at the discretion of the experimenter.

Bars 1, 2, and 3 (Fig. 5) are hollow with 0.062-in. wall thickness. Bar 1 contains the pressure taps and Bar 2 the thermocouples. Because of the influence of the thickness of these hollow bars in the calculation of the heat-transfer coefficients, the bars were made as accurate as possible within a tolerance of ±0.002 inches. Bar 3 was also made hollow because it is in contact with Bars 1 and 2, and the rest of the bars are solid. Bars 1, 2, and 3 were assembled by cementing together two parts that were mirror images. The model is held together by two thin plates, one at the top and one at the bottom (see Fig. 6), and two heavier pieces that fit snugly into steel "windows" in the two opposite wind-tunnel walls.

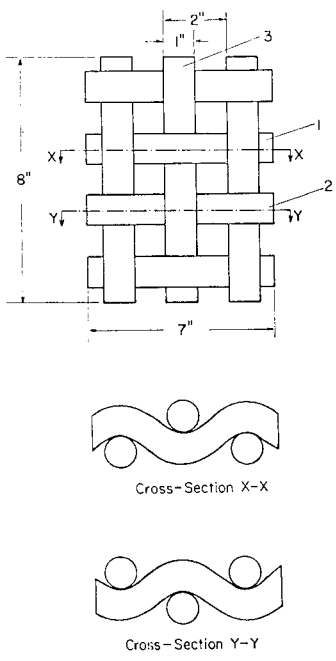

Fig. 5 Detailed sketch of the test model.

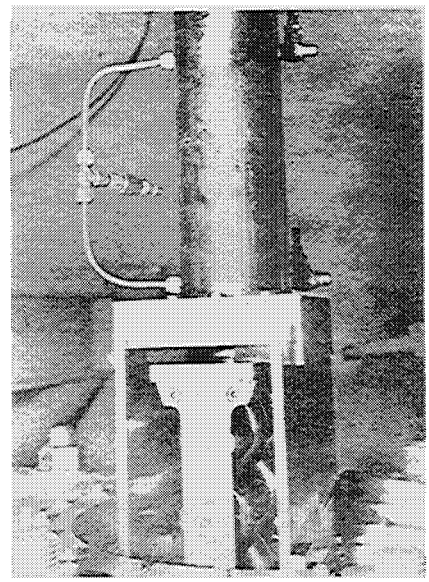

Fig. 6 Test model mounted in heating chamber.

With this construction, it was possible to retract the model from the wind tunnel (see Fig. 6) to heat it up to the desired temperature.

Measurements were taken at the six circular cross sections indicated in Fig. 7. The necessary information was obtained from five of these cross sections whereas the sixth, either *C-C* or *C'-C'*, served to check the symmetry of the flow. This symmetry is more apparent from Fig. 5 which shows the proximity of the instrumented bar with respect to all neighboring perpendicular bars. As mentioned previously, however, Bar 1 was instrumented only with pressure taps and Bar 2 only with thermocouples. Readings at all six cross sections shown in Fig. 6 were therefore obtained by rotating

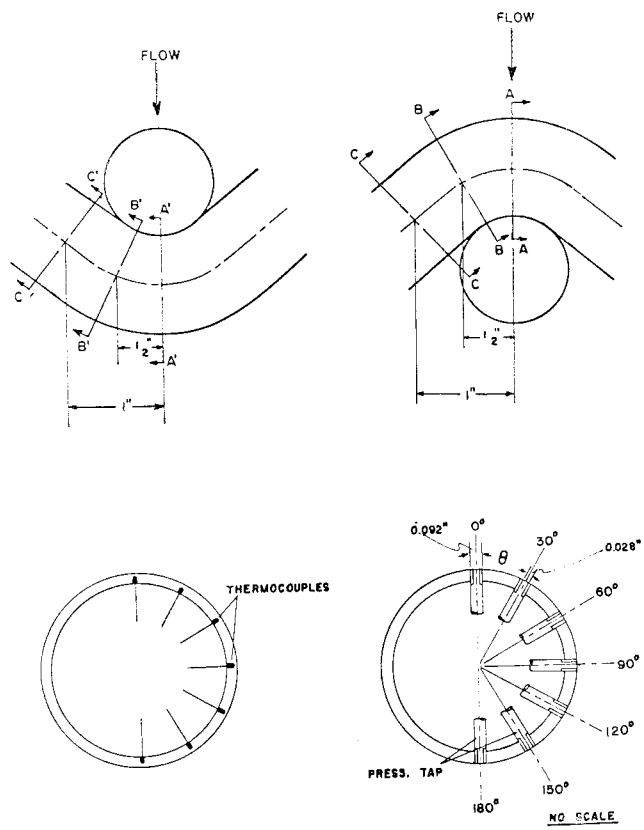

Fig. 7 Typical instrumentation of two cross sections corresponding to bars 2 and 1.

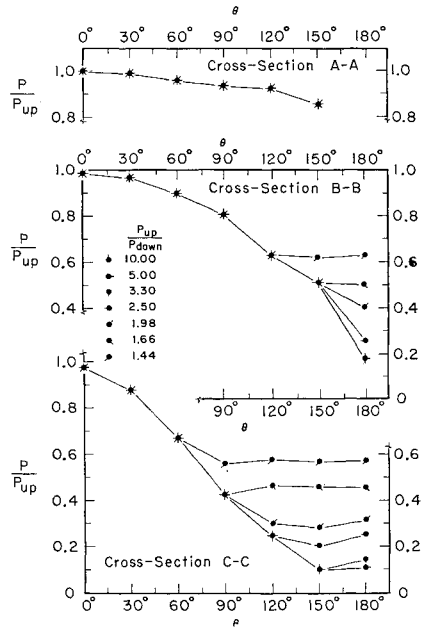

Fig. 8 Pressure distributions on the upstream surfaces of the mesh.

the model 180° and repeating the run. Thus cross sections *A-A*, *B-B*, and *C-C* are transformed into cross sections *A'-A'*, *B'-B'*, and *C'-C'*, respectively, by turning the model around.

The symmetry of the flow with respect to the horizontal axes *X-X* and *Y-Y*, respectively, shown in Fig. 7, made it necessary to place instrumentation around only half of the cross sections. The half cross sections instrumented were those farthest from the wind-tunnel walls. The cross-sections are instrumented at seven peripheral locations corresponding to the angles $\theta = 0°, 30°, 60°, 90°, 120°, 150°$, and 180° measured from the upstream side with the exception that in cross sections *A-A* and *A'-A'* there is no instrumentation at the point of contact. The pressure taps were silver-soldered in holes 0.028 in. in diameter and drilled in the wall (Fig. 7 gives a detailed explanation). The outside surface was repolished after this installation. All pressure taps were tested and found to be leakproof.

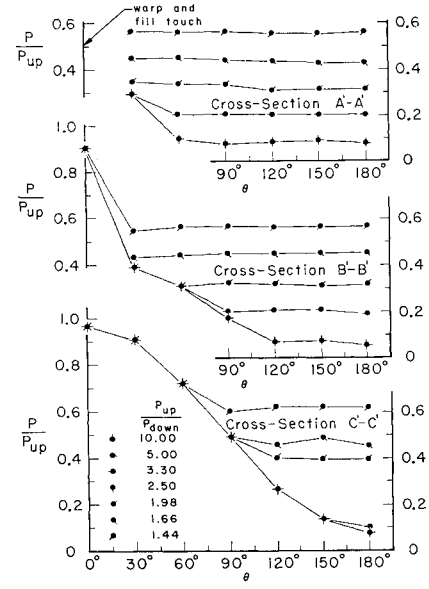

Fig. 9 Pressure distributions on the downstream surfaces of the mesh.

Thirty gage, roll-calibrated, iron-constantan thermocouples were inserted approximately $\frac{1}{32}$ in. in the wall of the model. After this the thermocouples were silver-soldered. The test model was mounted two nozzle heights downstream of the nozzle tangency point as shown in Fig. 3.

C. Heating Chamber

To carry out the heat-transfer measurements it was necessary to heat the model to a constant temperature before inserting it into the air stream. Figure 6 shows a view of the apparatus constructed to do this. The pneumatic piston in these figures made possible the insertion and removal of the model as fast as necessary. By regulating the valves it was possible to avoid destructive impacts against the wind-tunnel windows. The chamber exterior was built with removable top and bottom plates to facilitate handling of the heater. The heater consists of coiled Nichrome wire uniformly distributed on two removable asbestos plates placed on the side walls of the heating chamber. During the heating period the top plate was kept closed.

III. Experimental Results

A. Uniformity of Approach Flow

The approach flow velocities are within 1% of the centerline velocity with the exception of the four points taken near the nozzle walls. The latter points all yield low indicated velocities which are undoubtedly due to the nozzle boundary layers. The average approach velocity was found to be 134 fps. The uniformity of the approach flow seemed to be within tolerable limits.

B. Surface Pressure Distribution

The pressure distribution around the model in the cross sections *A-A*, *B-B*, and *C-C* was measured at different pressure ratios P_{up}/P_{down}. The model was then turned 180° around a horizontal axis through its midpoint, as explained in Sec. IIB, and the runs were repeated. In this case, the pressure distribution was measured at the cross sections *A'-A'*, *B'-B'*, and *C'-C'*.

Since the air was taken directly from the atmosphere through a piping system, the total pressure P_{up} varied only with the atmospheric conditions. One wall static-pressure tap located upstream (see Fig. 3), where the velocity of the

Fig. 10 Zones of separated flow.

air is negligible, gave $P_{up} \simeq P_{stag}$. Another wall static-pressure tap located in the centerline of the last window was used to measure P_{down}.

Figures 8 and 9 show the ratio P/P_{up} as a function of the angle θ, for the six cross sections. The almost constant pressure distribution around the cross section A-A, Fig. 8, can be explained by the fact that the flow is retarded by the presence of the rearward bar, thus causing the pressure to remain near the stagnation pressure. The scale is deceptive when one considers that the Mach number at $\theta = 30°$ is 0.14 at station A-A, 0.18 at station B-B, and 0.39 at station C-C. The remainder of the figures show that the pressure distribution around the upstream portion of the cross section is independent of pressure ratio up to a certain value of the angle θ, say θ_s. After separation, the pressure is nearly uniform.

Now the pressure distribution around a single isolated circular cylinder submersed in a two-dimensional ideal flow is given by

$$P/P_{up} = 1 - 4 \sin^2\theta[1 - (P_\infty/P_{up})] \qquad (2)$$

where P is the static pressure of the approaching flow of velocity v_∞. The term P/P_{up} (or the velocity v_∞) varies with the applied pressure ratio P_{up}/P_{down}. It is surprising that all of the pressure data are coincident for small θ. According to Eq. (2) the pure cylinder inviscid pressure ratio has a minimum at $\theta = 90°$ at rises to unity at the rear stagnation point. Cross section C-C more nearly approximates an infinite cylinder and slight rises are observed near $\theta = 90°$, followed by a region of constant pressure. A slight pressure rise is observed aft of the $\theta = 150°$ station. A recirculation zone forms downstream of the grid element. The reversed flow inside of the recirculation zone stagnates at the $\theta = 180°$ station and accelerates along the rear face of the cylinder toward the lesser angles.

When the grid is reversed with respect to the flow (the prime orientation—Fig. 9), a large portion of the flowfield lies in the wake of a vertical cross-member as is apparent in Fig. 10. This figure was constructed to give a visual display of the extensive regions of separated flow, as determined by the constant pressure regions of Figs. 8 and 9. It is clear that areas covered by separated flow (dotted) dominate the flow

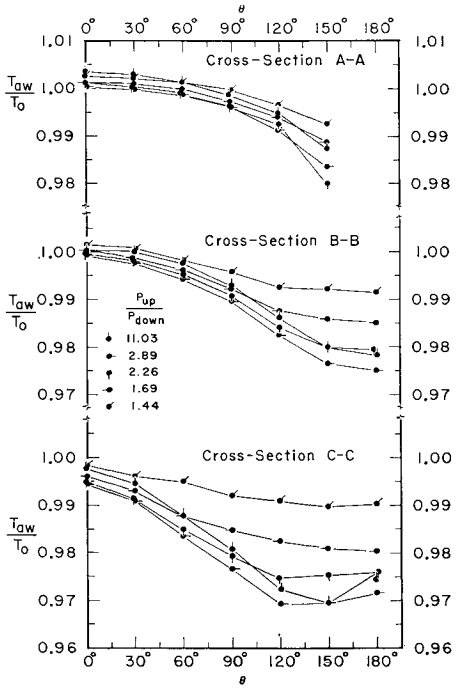

Fig. 11 Recovery temperature distributions on the upstream surfaces of the mesh.

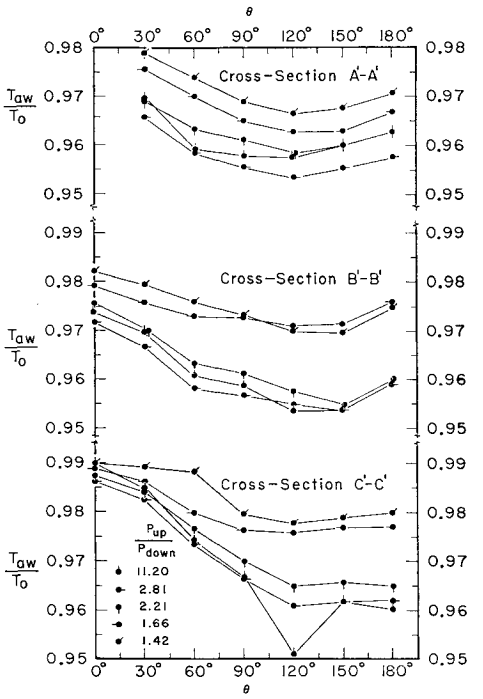

Fig. 12 Recovery temperature distributions on the downstream surfaces of the mesh.

patterns and that heat-transfer prediction methods based on attached flow situations must be viewed with caution.

C. Recovery Temperature Runs

The recovery temperature at each point around a surface is the temperature that this point assumes in steady state under the influence of internal friction in the boundary layer where the convective heat flux has the value zero. The ratio T_{aw}/T_0 of the absolute temperatures has been plotted as functions of the angle θ in Figs. 11 and 12. Cross sections A-A, B-B, and C-C indicated higher ratios of T_{aw}/T_0 at corresponding angles θ than cross sections A'-A', B'-B', and C'-C'. Cross sections C-C and $C'C'$ should show the same results. The difference may be attributable to a probable change of the relative humidity of the air, to the nonperfect symmetry of the flow, and to nonperfect alignment. The figures indicate that the temperature recovery is almost 100% over the upstream part of the model as well as in the separated flow regime.

D. Heat-Transfer Runs

Transient local heat-transfer data were taken in the cross sections mentioned. The technique required preheating the model with an electric heater to a temperature significantly different from the recovery temperature. To avoid circumferential heat conduction in the model, it was more important to obtain a uniform temperature distribution at the start o each run than to get a prescribed temperature. By observing the temperature readings during the heating period, it was possible to initiate the run when the temperatures were sufficiently uniform. In general, the model was heated to 250°F ± 5°. The conduction error in the heat-transfer coefficients produced by this difference was estimated and found negligible. Once the temperature distribution was uniform to this degree, the model was inserted in the wind tunnel in less than ½ sec. At the same time, two operators opened the upstream quick-opening DeZurik valve and the butterfly valve downstream between the wind tunnel and the vacuum tanks. In total, the system was operating in less than 1 sec. Owing to the rapid cooling of the grid upon insertion into the tunnel,

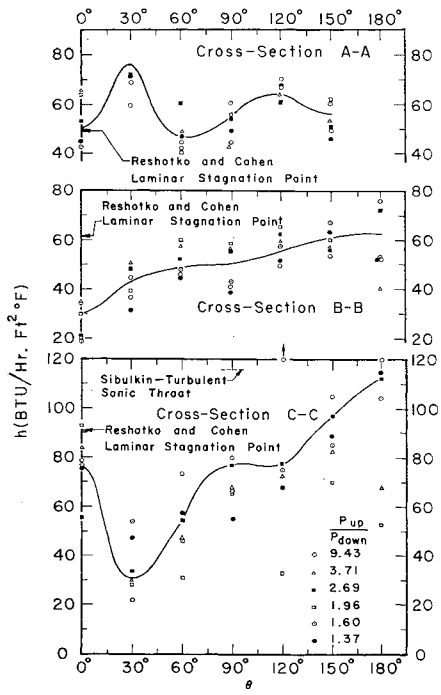

Fig. 13 Distribution of local heat-transfer coefficients on the upstream surfaces of the mesh.

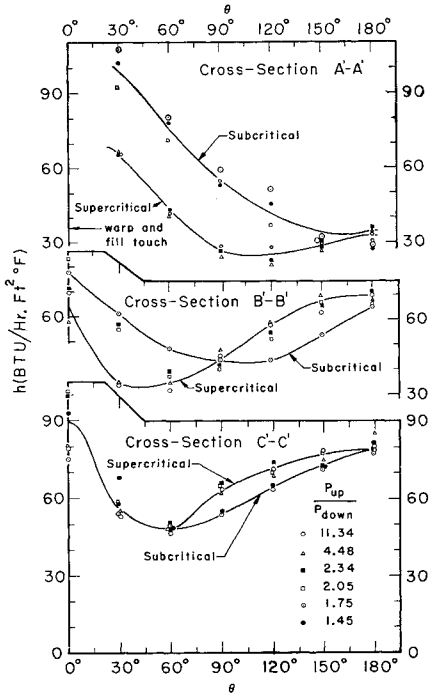

Fig. 14 Distribution of local heat-transfer coefficients on the downstream surfaces of the mesh.

rapid measurements of wall temperatures were necessary, and only one cross section was studied during each heat-transfer run. The heat-transfer coefficients were extrapolated to zero time ignoring data taken in the first second, since these data gave unreliable results arising from disturbances created by the actual insertion of the test grid. Data were taken at six different pressure ratios, three of them corresponding to supercritical pressure ratios, two to subcritical ratios, and the sixth one near the critical pressure ratio.

Local heat-transfer coefficients are presented in Figs. 13 and 14. The influence of the pressure ratio on heat transfer is somewhat puzzling. On the one hand, the pressure and recovery temperature distributions exhibit quite regular trends with pressure ratio, whereas both the pressure ratio and angular dependence of the heat-transfer coefficient are unclear. A discussion of some similar geometries seems to be in order here.

The flow around the front half of an isolated cylinder is accelerating and the boundary layer does not grow as rapidly as in the case of a flat plate. The boundary-layer thickness at $\theta = 90°$ is approximately twice the stagnation-point boundary-layer thickness. In a supersonic nozzle the accelerations are so rapid that the boundary layers have minimum thickness and maximum heat flux rates at the nozzle throat, since the heat-transfer coefficient is proportional to k/δ where δ is the film thickness.

The laminar stagnation point predictions of Reshotko and Cohen[9] are given in Fig. 13 for the forward stagnation line.¶ The velocity gradients were found using Figs. 8 and 9. Clearly, the stagnation point velocity gradient increases sharply from A to C.

Since the upstream total pressure was close to atmospheric, the upstream conditions are constant for supercritical operations and there should be no effect of pressure ratio. The observed scatter on the foreward-facing surfaces is apparently not due to installation errors since when the model orientation is reversed the trends are regular (Fig. 14).

¶ The measured gradient at point A was found to be 13% greater than the value computed from the relation $C = 2U_\infty/R$.

For supercritical pressure ratios the $\theta = 90°$ station at section C-C closely approximates the sonic point location and one looks for a heat-transfer maximum at this point. The data indicate a relative maximum followed by further increases. The nominal Reynolds number Re^*_D is 500,000, indicating a good possibility that boundary-layer transition has occurred aft of the $\theta = 30°$ station. With this in mind, the Sibulkin prediction[10] for a turbulent boundary layer in a sonic throat is given in Fig. 13 for reference.

For the rearward-facing instrumentation runs the data separate according to the critical pressure ratio condition. The grouping is especially clear for section C'-C', which is really a repeat of C-C, only in the first case the stagnation point prediction is closely matched by the data. An engineering conclusion is that there are no large variations of heat flux around the body and that the conventional laminar stagnation point prediction is useful as a first approximation.

The conventional expressions for laminar heat transfer contain the body dimension to nearly the minus one-half power. For a nonporous parachute this dimension would be related to the over-all parachute radius R, whereas for the case of an intermediate porosity parachute this dimension would be the mesh radius r, regardless of whether individual shocks would exist over each fiber. As pointed out in Ref. 1, the heat transfer in the latter case would be larger by the factor $(R/r)^{1/2}$ than the former. Even a small amount of porosity will increase the heat-transfer rate to a porous fibrous structure.

Conclusions

Experiments have been performed to determine the local pressure and heat-transfer distributions on an individual fiber of a porous parachute with a geometric porosity of 25%. The pressure ratio applied across the mesh was considered as the primary variable and was varied from subcritical (1.45) to supercritical (11) values. The unit Reynolds number Re_D^* was held constant at 5×10^5. The upstream total pressure was atmospheric.

The experiments show that the local pressure and heat flux values are generally independent of the applied pressure ratio

for the windward-facing surfaces when the flows are attached. Regions of separated flow covered approximately 70% of the surface area exposed to the flow. In the sheltered regions the sub- and supercritical pressure ratios produced two distinct behavior patterns. Measurements of recovery temperatures show only a small influence of pressure ratio on the recovery factor.

There are no large variations of heat flux over the surfaces of the mesh. The data agree with conventional laminar boundary-layer stagnation point predictions, a fact that is convenient for predicting the thermal response of actual parachutes.

References

[1] Hritzay, D. and Wiant, R., "Wire Cloth Structure for a Radiating Re-Entry Vehicle," Research Rept. 123, March 1962, Avco-Everett Research Lab., Everett, Mass.

[2] Kyser, A. C., "The Rotornet: A High-Performance Hypersonic Decelerator for Planetary Entry," CR-247, June 1965, NASA.

[3] Koh, J. C. Y. and Hartnett, J. P., "Measured Pressure Distribution and Local Heat Transfer Rates for Flow over Concave Hemispheres," *ARS Journal*, Vol. 31, No. 1, Jan. 1961, pp. 71–75.

[4] Korst, H. H., Chow, W. L., and Zumwalt, G. W., "Research on Transonic and Supersonic Flow of a Real Fluid at Abrupt Increases in Cross Section (Final Report)," TR 392-5, Dec. 1959, University of Illinois, Engineering Experiment Station.

[5] Herman, R., "Problems of Hypersonic Flight at the Re-Entry of Satellite Vehicles," RAL-RR-153, Nov. 1958, University of Minnesota, Rosemount Aeronautical Laboratories.

[6] Domich, E. G., Jantscher, H. N., and Olson, D. N., "Aeronautical Research Facilities," RAL-RR-152, Sept. 1958, University of Minnesota, Rosemount Aeronautical Laboratories.

[7] Baines, W. D. and Peterson, E. G., "An Investigation of Flow through Screens," Rept. 2, July 1949, Iowa Institute of Hydraulic Research.

[8] Rouse, H. and Hasson, M. M., "Cavitation-Free Inlets and Contractions," *Mechanical Engineering*, March 1949.

[9] Reshotko, E. and Cohen, C. B., "Heat Transfer at the Forward Stagnation Point of Blunt Bodies," TN 3513, 1955, NACA.

[10] Sibulkin, M., "Heat Transfer to an Incompressible Turbulent Boundary Layer and Estimation of Heat-Transfer Coefficients at Supersonic Nozzle Throats," *Journal of the Aerospace Sciences*, Vol. 23, No. 2, Feb. 1956, pp. 162–72.